Journal of Sound and Vibration (2001) **244**(5), 795–820
doi:10.1006/jsvi.2000.3535, available online at http://www.idealibrary.com on IDEAL®

BIFURCATION AND STABILITY ANALYSES FOR A COUPLED BRUSSELATOR MODEL

P. YU

Department of Applied Mathematics, University of Western Ontario, London, Ontario, Canada N6A 5B7.
E-mail: pyu@pyu1.apmaths.uwo.ca

AND

A. B. GUMEL

Department of Mathematics, University of Manitoba, Winnipeg, Manitoba, Canada R3T 2N2

(*Received* 3 *July* 2000, *and in final form* 20 *November* 2000)

This paper addresses the dynamic behaviour of a chemical oscillator arising from the series coupling of two Brusselators. Of particular interest is the study of the associated Hopf bifurcation and double-Hopf bifurcations. The motion of the oscillator may either be periodic (bifurcating from a Hopf-type critical point), or quasi-periodic (bifurcating from a compound critical point). Furthermore, bifurcation analysis reveals that the limit cycles associated with the first Brusselator are always stable, while that generated by the second Brusselator may be unstable if the parameter values are chosen far from the stability boundary. It is interesting to note that in the vicinity of the double-Hopf compound critical point, there exist periodic as well as quasi-periodic solutions. The quasi-periodic motion is stable for a small parameter region. A robust Gauss–Seidel like implicit finite-difference method (GS1) has been developed and used for the solution of the resulting initial-value problem (IVP). In addition to being of comparable accuracy (judging by the similarity of the profiles generated) with the fourth order Runge–Kutta method (RK4), the GS1 method will be seen to have better numerical stability property than RK4. Unlike the RK4, which fails when large time steps are used to integrate the IVP, extensive numerical simulations with appropriate initial data suggest that the GS1 method is unconditionally convergent. Moreover, it is more economical computationally.

© 2001 Academic Press

1. INTRODUCTION

It is well known that many chemical systems often exhibit oscillations; and thus the study of the stability of these systems is important [1, 2]. One of the most widely studied non-linear oscillators is the Brusselator system given by [1–4]

$$A \to X, \qquad B + X \to Y + D, \qquad 2X + Y \to 3X, \qquad X \to E, \tag{1}$$

where A and B are input chemicals, D and E are output chemicals and X and Y are intermediates. It is known [4] that the trimolecular reaction step described by the third equation of equation (1) arises in the formation of ozone by atomic oxygen *via* a triple collision, enzymatic reactions, and in plasma and laser physics in multiple couplings between modes.

0022-460X/01/300795 + 26 $35.00/0 © 2001 Academic Press

Many researchers have studied the ability of non-linear oscillators to synchronize to external influences. This provides the basis for analytical investigations of multiple oscillations in a chemical network. To better understand the complex dynamics associated with such systems, Tyson [3] proposed a model consisting of two Brusselators coupled in series in which two outputs to the first provide the two inputs of the second, described by

$$A \to X, \qquad B + X \to Y + U, \qquad 2X + Y \to 3X, \qquad X \to E,$$
$$E + U \to V + F, \qquad 2U + V \to 3U, \qquad U \to G. \tag{2}$$

Bifurcation and stability analysis on coupled oscillators has been an interesting topic for several decades and many results have been reported in the literature (see, for instance, reference [5–13]). Recently, the double-pendulum system has been reinvestigated in detail to show that such a system can indeed exhibit rich dynamical behaviour, in the vicinity of various compound critical points [14].

In this paper, analytical and numerical approaches are employed to solve a coupled Brusselator model. Three different types of bifurcations emerged from the associated (unique) equilibrium point, namely, Hopf bifurcation corresponding to the first oscillator, Hopf bifurcation corresponding to the second oscillator, and double-Hopf bifurcation due to the interaction of the two modes. Two families of limit cycles are generated from the two Hopf bifurcations, while secondary bifurcations from the Hopf bifurcations may lead to quasi-periodic solutions which represent motions on a family of two-dimensional tori. Centre manifold theory [15] and normal form theory [5, 6, 16–18] were used to simplify the theoretical analyses. In particular, the symbolic computer programs developed in references [19–21] for computing normal forms using Maple were adapted and used to obtain bifurcation solutions and their associated stability conditions explicitly. Moreover, expressions for the critical boundaries, along which incipient and secondary bifurcations leading to limit cycles and two-dimensional tori occur, were derived.

It is known that discretizing ODEs by explicit Euler or Runge–Kutta finite-difference schemes can result in contrived chaos whenever the discretization parameters exceed certain values (see reference [22]). Although chaos can often be avoided, even for Euler and Runge–Kutta methods, by using small time steps, the extra computing costs incurred when examining the long-term behaviour of a dynamical system may be substantial. It is therefore desirable to use a numerical method which allows the largest possible time steps that are consistent with stability and accuracy. To avoid contrived chaos, whilst retaining accuracy and numerical stability, it may be necessary to forego the ease-of-implementation of inexpensive explicit numerical methods in favour of implicit methods (which are, at times, computationally intensive).

In the current study, a new Gauss–Seidel like first order implicit finite-difference method has been developed for the solution of the associated IVP. In addition to its superior stability and convergence properties in comparison with some existing numerical methods, this new method is easy to implement and has a fast convergence rate (as expected of Gauss–Seidel-type methods).

Extensive numerical simulations were carried out using both the RK4 and the GS1 methods [23]. These experiments revealed that the GS1 method not only gives comparable numerical results (of similar accuracy) with the RK4 method, but is also computationally efficient and robust. For instance, unlike the RK4 method, which fails when large time steps are used to integrate the IVP, extensive numerical simulations suggest that the GS1 is unconditionally convergent for appropriate choices of parameter and initial values.

However, it was also found that when simulating the dynamic (periodic or quasi-periodic) solutions, the GS1 method, unlike the RK4 method, may lose its stability if the dynamic solution is very sensitive to initial conditions.

In section 2, a detailed static analysis is given for the associated equilibrium point together with its stability conditions. Section 3 is devoted to the analytical study of the coupled Brusselator, and section 4 presents the numerical simulation results. Finally, conclusions are drawn in section 5.

2. SYSTEM EQUATIONS AND STATIC ANALYSIS

Consider the kinetic equations associated with equation (2), given by Tyson [3]

$$\begin{aligned}
\dot{z}_1 &= f_1(\mathbf{z}, A, B) = A - Bz_1 + z_1^2 z_2 - z_1,\\
\dot{z}_2 &= f_2(\mathbf{z}, A, B) = Bz_1 - z_1^2 z_2,\\
\dot{z}_3 &= f_3(\mathbf{z}, A, B) = z_1 - z_3 z_4,\\
\dot{z}_4 &= f_4(\mathbf{z}, A, B) = Bz_1 - z_3 z_4 + z_4^2 z_5 - z_4,\\
\dot{z}_5 &= f_5(\mathbf{z}, A, B) = z_3 z_4 - z_4^2 z_5,
\end{aligned} \tag{3}$$

where $\mathbf{z} = (z_1, z_2, z_3, z_4, z_5)^{\mathrm{T}} = (X, Y, E, U, V)^{\mathrm{T}}$, A and B are real constants, and the overdot denotes the differentiation with respect to time t. It is easy to show that the only equilibrium of the system, determined by setting $\dot{\mathbf{z}} = \mathbf{f} = \mathbf{0}$, is

$$\mathbf{z}_c = \left(A, \frac{B}{A}, \frac{1}{B}, AB, \frac{1}{AB^2} \right)^{\mathrm{T}}. \tag{4}$$

Applying the translation $\mathbf{z} = \mathbf{y} + \mathbf{z}_c$ to equation (3) yields

$$\begin{aligned}
\dot{y}_1 &= (B-1)y_1 + A^2 y_2 + \frac{B}{A} y_1^2 + 2Ay_1 y_2 + y_1^2 y_2,\\
\dot{y}_2 &= -By_1 - A^2 y_2 - \frac{B}{A} y_1^2 - 2Ay_1 y_2 - y_1^2 y_2,\\
\dot{y}_3 &= y_1 - ABy_3 - \frac{1}{B} y_4 - y_3 y_4,\\
\dot{y}_4 &= By_1 - ABy_3 + \left(\frac{1}{B} - 1 \right) y_4 + A^2 B^2 y_5 + \frac{1}{AB^2} y_4^2 - y_3 y_4 + 2ABy_4 y_5 + y_4^2 y_5,\\
\dot{y}_5 &= ABy_3 - \frac{1}{B} y_4 - A^2 B^2 y_5 - \frac{1}{AB^2} y_4^2 + y_3 y_4 - 2ABy_4 y_5 - y_4^2 y_5.
\end{aligned} \tag{5}$$

Then the unique equilibrium of system (5) is $\mathbf{y} = \mathbf{0}$, and the characteristic polynomial of the linearized system evaluated at the equilibrium can be found as

$$[\lambda^2 + (A^2 - B + 1)\lambda + A^2]$$

$$\times\left[\lambda^3 + \left(A^2B^2 + AB + 1 - \frac{1}{B}\right)\lambda^2 + (A^3B^3 + A^2B^2 + AB - 2A)\lambda + A^3B^3\right] = 0. \quad (6)$$

The two factors correspond to the first and second oscillators respectively. In order for the equilibrium, $\mathbf{y} = \mathbf{0}$, to be stable, the conditions

$$g_1 = A^2 - B + 1 > 0, \quad A \neq 0 \quad (7)$$

and

$$g_2 = A^2B^2 + AB + 1 - \frac{1}{B} > 0,$$

$$g_3 = A^3B^3 + A^2B^2 + AB - 2A > 0,$$

$$g_4 = A^3B^3 > 0, \text{ i.e., } AB > 0,$$

$$g_5 = \left(A^2B^2 + AB + 1 - \frac{1}{B}\right)(A^3B^3 + A^2B^2 + AB - 2A) - A^3B^3 > 0, \quad (8)$$

must be satisfied. Our focus here is to, first of all, discuss the stability of the two oscillators separately, and then combine them to obtain the general (dynamical) picture. Suppose that the parameters A and B are real and positive, as is the case for any chemical system. When condition (7) is satisfied, it defines a region in the parameter A–B space under the curve g_1 but excluding the B-axis, where the first Brusselator is stable (see Figure 1). If the parameters A and B are changed such that the B-axis (i.e., $A = 0$) is first crossed, then a static bifurcation may occur; while when the curve g_1 is crossed first, a Hopf bifurcation occurs, leading to self-excited periodic vibration of the first oscillator.

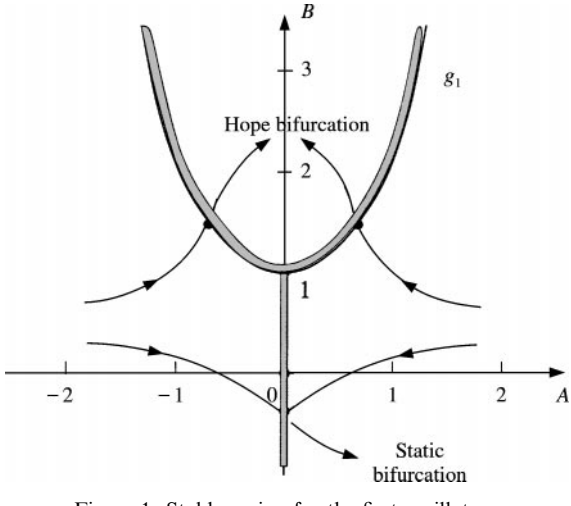

Figure 1. Stable region for the first oscillator.

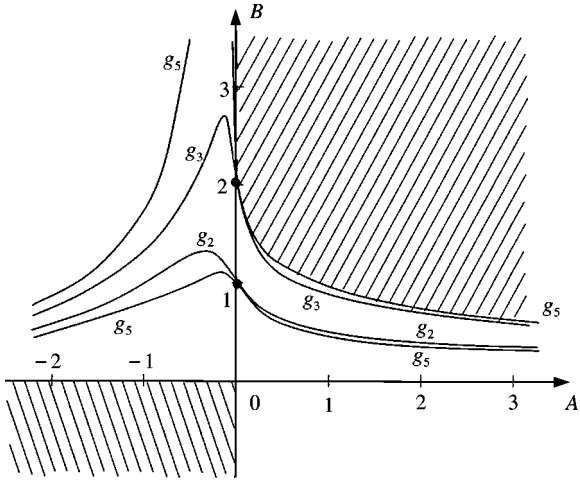

Figure 2. Stable region for the second oscillator.

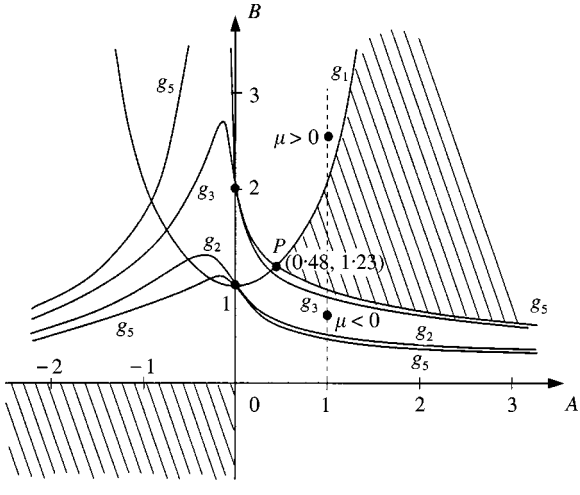

Figure 3. Stable region for the equilibrium.

Consider, now, the conditions given in equation (8), which define the stable region for the second oscillator (depicted in Figure 2). It is easy to observe that Figure 2 indicates the possibility of having both static and Hopf bifurcations. The static bifurcation occurs when the parameters are varied to cross the B-axis from the stable region, while the Hopf bifurcation results when the curve g_5 is first crossed. Note that the A-axis (i.e., $B = 0$) is excluded from the stability boundaries.

Now combine the stability regions shown in Figures 1 and 2 for the first and second oscillators, respectively, to obtain the stable region for the equilibrium $\mathbf{y} = \mathbf{0}$, as shown in Figure 3. There are two parts: one part is the third quadrant excluding the A- and B-axis, and the other part is located in the first quadrant bounded by the curves g_1 and g_5 which intersect at the critical point P (0·48, 1·23).

If the real constants A and B are restricted as non-negative real values (as before), then only the part located in the first quadrant needs to be considered. It is easy to observe the routes to bifurcations from Figure 3. Suppose that the system's parameters A and B are

initially chosen from the shadowed region located in the first quadrant of Figure 3; then the system (or the equilibrium state) is stable. There exist only two possibilities which may violate the stability conditions for the equilibrium: the parameters are varied so that either the curve g_1 is crossed first, where a Hopf bifurcation occurs, corresponding to the first oscillator, or the curve g_5 is crossed, resulting in yet another Hopf bifurcation (corresponding to the second oscillator). An interesting point is the critical point P where a double-Hopf bifurcation may occur, corresponding to the simultaneous excitation of the oscillating modes [5, 6, 10, 14].

Based on the above discussion, we propose the following three possible models for the bifurcations from the equilibrium point $\mathbf{y} = \mathbf{0}$.

Case (1) If the parameters A and B are chosen too close to the stability boundary g_1, then we have a bifurcation model corresponding to the first Brusselator oscillator. This oscillator is independent of the second Brusselator, but the second Brusselator is coupled with the first Brusselator. In other words, there is one-way coupling between the two oscillators. Therefore, even when the second oscillator is stable, it may be excited to exhibit vibrations due to the coupling. The bifurcation and stability analysis are completely determined by the first two equations of equation (5).

Case (2). If the parameters A and B are chosen too close to the stability boundary g_5, then we have a bifurcation model corresponding to the second Brusselator. Unlike in Case (1) above, however, this oscillator is not independent from the first Brusselator. Therefore, the bifurcation and stability analysis cannot be carried out on the basis of the last three equations of equation (5). Since on the stability boundary g_5, the eigenvalues of the whole system have a purely imaginary pair and the remaining three eigenvalues have negative real parts, we may apply centre manifold theory to obtain a two-dimensional manifold which includes the influence from the first oscillator.

Case (3). If the parameters A and B are chosen too close to the critical point P, then we must establish a double-Hopf bifurcation model. Otherwise, the associated complex dynamic behaviour of the system (such as quasi-periodic solutions or chaos) may not be observed if single-Hopf bifurcation model (either the first or the second oscillator) is used. In this case, the model is of codimension two [5, 10] and we should use both A and B as independent bifurcation parameters.

3. ANALYSIS OF THE DYNAMICAL SYSTEM

In this section, we shall use normal form theory as well as centre manifold theory to consider the possible dynamic behaviour that the coupled Brusselator system, given by equation (6), may exhibit. Three models will be established for the purpose of bifurcation and stability analyses.

3.1. MODEL (I): HOPF BIFURCATION (THE FIRST OSCILLATOR)

First, consider Case (1) in which periodic solutions bifurcate from a critical point located on the boundary g_1 (in the first quadrant, but not close to the critical point P). Then the first Brusselator is decoupled from the second Brusselator and the first two equations of equation (5) represent the centre manifold and the last three equations make no contribution to the centre manifold. Thus, we may, instead of using the whole system (5), consider only the first two equations of equation (5), and then apply normal form theory for Hopf bifurcation [5, 6, 16–19] to the system to obtain the following normal form given in

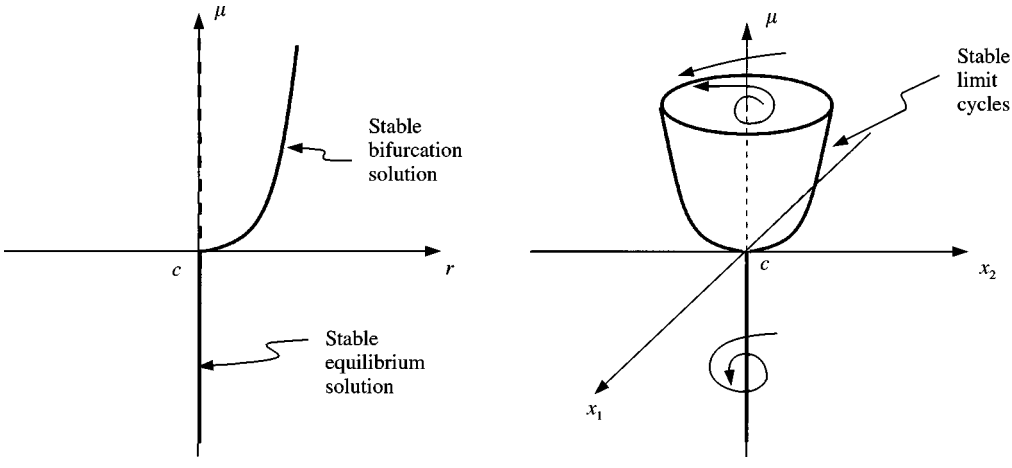

Figure 4. Bifurcation diagram for Model (I).

the polar co-ordinates:

$$\dot{r} = \frac{1}{2} A\mu r - \frac{2 + A^2}{8(1 + A^2)} r^3, \qquad \dot{\theta} = A - \frac{4A^4 - 7A^2 + 4}{24A(1 + A^2)} r^2, \tag{9}$$

where $\mu = B - (1 + A^2)$, treated as a small bifurcation parameter, and r and θ are the amplitude and the phase of the periodic motion respectively.

Now, based on equation (9), bifurcation solutions and their stability conditions can be easily obtained. In fact, the first equation of equation (9) is sufficient in deriving the solution of a family of limit cycles together with the stability conditions. The second equation of equation (9) gives information on the frequency of the bifurcating periodic solutions.

Setting $\dot{r} = 0$ in equation (9) results in two steady state solutions:

$$\text{(a) } r = 0, \qquad \text{(b) } r^2 = \frac{4A(1 + A^2)}{2 + A^2} \mu. \tag{10}$$

Solution (10a), $r = 0$, in fact, represents the initial equilibrium solution $y_1 = y_2 = 0$. When $A > 0$, the bifurcating periodic solution (10b) exist for $\mu > 0$.

The stability of the steady state solutions is determined by the Jacobian of the first equation of equation (9), $J = (\mathrm{d}/\mathrm{d}r)(\mathrm{d}r/\mathrm{d}t) = \mathrm{d}\dot{r}/\mathrm{d}r$. When $J < 0$ (>0), the solution is stable (unstable). A simple calculation indicates that when $\mu < 0$ (i.e., $B < 1 + A^2$), the equilibrium ($r = 0$) is stable. When μ is varied to cross the critical point $\mu_c = 0$ (i.e., $B = 1 + A^2$) and becomes positive ($\mu > 0$, i.e., $B > 1 + A^2$), the equilibrium loses stability and bifurcates into a family of periodic solutions described by solution (10b).

For the periodic solution (10b), it is shown that when $\mu > 0$ ($A > 0$), the Hopf bifurcation is *supercritical*, i.e., the periodic solution given by (10b) is always stable for $\mu > 0$. The bifurcation diagram and periodic solutions are depicted in Figure 4.

3.2. MODEL (II): HOPF BIFURCATION (THE SECOND OSCILLATOR)

In this case, a critical point is chosen from the boundary g_5, where another family of limit cycles bifurcates from the equilibrium $\mathbf{y} = \mathbf{0}$. However, unlike the analysis for Model (I), we

cannot obtain a closed-form solution for A or B from equation $g_5 = 0$, since it gives either a fifth or sixth degree polynomial. Therefore, we must use numerical values of A and B in finding the normal forms for this Model. The dynamic behaviour of the system can be studied using the following mechanism: first of all, choose an arbitrary value of $A > 0$, and solve $g_5 = 0$ to obtain a critical value B_c, and then give a perturbation to B in the form of $B = B_c + \mu$, where μ is a small perturbation parameter. Next, apply centre manifold theory to find a two-dimensional centre manifold and finally, employ normal form theory to obtain the explicit expression of the normal form on the centre manifold.

For instance, consider $A = 1$. Solving $g_5 = 0$ then yields a real root $B_c = 0{\cdot}903478$. It should be noted that $g_5 = 0$ gives multiple roots, and one should choose the largest real positive root which is located on the boundary g_5 (see Figure 3). Next let $B = 0{\cdot}903478 + \mu$, and $\mu = 0$ corresponds to the critical point $(A, B) = (1{\cdot}0, 0{\cdot}903478)$. Substituting $A = 1$ and $B = 0{\cdot}903478 + \mu$ into equation (5) and then evaluating the Jacobian of the system on the equilibrium $\mathbf{y} = \mathbf{0}$ yields the following eigenvalues: one purely imaginary pair $\pm 0{\cdot}676193i$, one real $-1{\cdot}612918$ and a complex conjugate $-0{\cdot}548261 \pm 0{\cdot}836307i$. Therefore, similar to Model (I), one can apply the centre manifold theory and the normal form theory [5, 6, 16–19] to find the normal form given in polar co-ordinates:

$$\dot{r} = -1{\cdot}286789r\mu - 0{\cdot}042734r^3, \qquad \dot{\theta} = 0{\cdot}676193 + 0{\cdot}816930\mu - 0{\cdot}024482r^2. \quad (11)$$

A bifurcation analysis similar to that given for Model (I) can be applied for this case. However, it should be noted that for Model (I), a negative value of μ is located in the stable region of the initial equilibrium, while here (in Model II), a positive value of μ is located in the stable region. Therefore, we should consider bifurcations when μ is varied from positive to negative. This can be observed from the vertical dotted line which passes through the point $A = 1$ (see Figure 3). The results are summarized below: the steady state solutions are

$$\begin{aligned} &\text{(a) } r = 0 \quad \text{(initial equilibrium)},\\ &\text{(b) } r^2 = -30{\cdot}111522\mu \quad \text{(periodic solution)} \end{aligned} \quad (12)$$

and their stability conditions are given by

$$\text{Equilibrium (a)} \begin{cases} \text{Stable}, & \text{when } \mu > 0,\\ \text{Unstable}, & \text{when } \mu < 0 \end{cases} \quad (13)$$

and

$$\text{Periodic solution (b)} \begin{cases} \text{Does not exist}, & \text{when } \mu > 0,\\ \text{Stable}, & \text{when } \mu < 0 \end{cases} \quad (14)$$

respectively. The bifurcation diagram is similar to Figure 4 and thus omitted, but it should be noted that the parameter μ should be varied from positive to negative (reserving the arrow of the μ-axis).

In Table 1, we list the results for different values of A from 0·8 to 7·0. It is seen that for all the different values of A, the equilibrium loses stability at $\mu = 0$, and changes from stable to unstable when the μ is varied from positive to negative. This can be clearly observed from Figure 4 (that is, the equilibrium moves along the vertical dotted line from the stable region to unstable region). However, unlike Model (I), where the bifurcating periodic solutions are always stable, here the limit cycles change stability at a critical point $A_h = 6{\cdot}046327$. When $A < (>) A_h$, the bifurcating limit cycle is stable (unstable).

TABLE 1

Bifurcation solutions for Model (II)

A	B_c	Normal form	Solution	Stability
0·8	1·001074	$\dot{r} = -0{\cdot}980373r\,\mu - 0{\cdot}126392r^3$ $\dot{\theta} = 0{\cdot}596561 + 0{\cdot}662730\mu - 0{\cdot}058015r^2$	$r = 0$ $r^2 = -7{\cdot}756584\mu$	S: $\mu > 0$, U: $\mu < 0$ S: $\mu < 0$
0·9	0·949154	$\dot{r} = -1{\cdot}131249r\,\mu - 0{\cdot}162160r^3$ $\dot{\theta} = 0{\cdot}638215 + 0{\cdot}740638\mu - 0{\cdot}082818r^2$	$r = 0$ $r^2 = -6{\cdot}976141\mu$	S: $\mu > 0$, U: $\mu < 0$ S: $\mu < 0$
1·0	0·903478	$\dot{r} = -1{\cdot}286789r\,\mu - 0{\cdot}042734r^3$ $\dot{\theta} = 0{\cdot}676193 + 0{\cdot}816930\mu - 0{\cdot}024482r^2$	$r = 0$ $r^2 = -30{\cdot}11152\mu$	S: $\mu > 0$, U: $\mu < 0$ S: $\mu < 0$
1·5	0·737696	$\dot{r} = -2{\cdot}120831r\,\mu - 0{\cdot}075679r^3$ $\dot{\theta} = 0{\cdot}828179 + 1{\cdot}177633\mu - 0{\cdot}073857r^2$	$r = 0$ $r^2 = -28{\cdot}02389\mu$	S: $\mu > 0$, U: $\mu < 0$ S: $\mu < 0$
2·0	0·632296	$\dot{r} = -3{\cdot}025811r\,\mu - 0{\cdot}361801r^3$ $\dot{\theta} = 0{\cdot}941335 + 1{\cdot}509680\mu - 0{\cdot}538460r^2$	$r = 0$ $r^2 = -8{\cdot}363191\mu$	S: $\mu > 0$, U: $\mu < 0$ S: $\mu < 0$
3·0	0·503182	$\dot{r} = -4{\cdot}979681r\,\mu - 0{\cdot}525145r^3$ $\dot{\theta} = 1{\cdot}108202 + 2{\cdot}107220\mu - 1{\cdot}544250r^2$	$r = 0$ $r^2 = -9{\cdot}482482\mu$	S: $\mu > 0$, U: $\mu < 0$ S: $\mu < 0$
5·0	0·372230	$\dot{r} = -9{\cdot}247669r\,\mu - 0{\cdot}0900342r^3$ $\dot{\theta} = 1{\cdot}331097 + 3{\cdot}107997\mu - 1{\cdot}206721r^2$	$r = 0$ $r^2 = -102{\cdot}7128\mu$	S: $\mu > 0$, U: $\mu < 0$ S: $\mu < 0$
6·046327 (A_h)	0·331776	$\dot{r} = -11{\cdot}605807r\,\mu - 0{\cdot}000000r^3$ $\dot{\theta} = 1{\cdot}417762 + 3{\cdot}554365\mu - 0{\cdot}455397r^2$	$r = 0$ Not determined	S: $\mu > 0$, U: $\mu < 0$
7·0	0·303357	$\dot{r} = -13{\cdot}808860r\,\mu + 0{\cdot}026177r^3$ $\dot{\theta} = 1{\cdot}485998 + 3{\cdot}924694\mu - 0{\cdot}506325r^2$	$r = 0$ $r^2 = 527{\cdot}5268\mu$	S: $\mu > 0$, U: $\mu < 0$ U: $\mu < 0$

3.3. MODEL (III): DOUBLE-HOPF BIFURCATION

For this case, the critical point is the point P (see Figure 3) where $A = 0{\cdot}479012$ and $B = 1{\cdot}229453$ at which the Jacobian of system (5) has two pairs of purely imaginary eigenvalues: $\lambda_{1,2} = \pm 0{\cdot}426596i$, $\lambda_{3,4} = \pm 0{\cdot}479012i$ and a real eigenvalue $\lambda_5 = -1{\cdot}122382$. We may consider the two modes as non-resonant because the ratio of the two frequencies is $0{\cdot}479012/0{\cdot}426596 = 1{\cdot}122870$. Since near this critical point, the system is of codimension two, we need to use two perturbation parameters [5, 6]. Thus, we choose both A and B as the perturbation parameters and let

$$A = 0{\cdot}479012 + \mu_1 \quad \text{and} \quad B = 1{\cdot}229453 + \mu_2. \tag{15}$$

Then the eigenvalues of the system evaluated at the equilibrium $\mathbf{y} = \mathbf{0}$ are $\pm 0{\cdot}426596i$, $\pm 0{\cdot}479012i$ and $-1{\cdot}122382$. After applying the centre manifold theory and the normal form theory to the system, one may obtain the following normal form given in the polar co-ordinates [20, 21]:

$$\begin{aligned} \dot{r}_1 &= -r_1[0{\cdot}487023\mu_1 + 0{\cdot}534819\mu_2 + 0{\cdot}153084r_1^2 + 0{\cdot}071469r_2^2], \\ \dot{r}_2 &= -r_2[0{\cdot}479012\mu_1 - 0{\cdot}5\mu_2 + 0{\cdot}007462r_2^2] \end{aligned} \tag{16}$$

and

$$\begin{aligned} \dot{\theta}_1 &= 0{\cdot}426596 + 1{\cdot}012126\mu_1 + 0{\cdot}399767\mu_2 - 0{\cdot}126129r_1^2 - 0{\cdot}051774r_2^2, \\ \dot{\theta}_2 &= 0{\cdot}479012 + \mu_1 - 0{\cdot}006066r_2^2. \end{aligned} \tag{17}$$

The steady state solutions and their stability conditions can be derived from equation (16). Furthermore, bifurcation routes of the system can also be found from equation (16). Guckenheimer [5] has given a detailed classification for codimension two bifurcation problems. For the coupled double-Brusselator model, we may apply the results given in reference [5] or use the explicit formulas derived in reference [10] to obtain expressions for the bifurcation solutions, their stability conditions as well as bifurcation boundaries.

The steady state solutions are obtained by setting $\dot{r}_1 = \dot{r}_2 = 0$ as follows:

(1) The initial equilibrium solution (ES):

$$r_1 = r_2 = 0 \quad (\text{i.e., } y_i = 0); \tag{18}$$

(2) Hopf bifurcation solution (HB (I) with frequency ω_1):

$$\begin{aligned} r_1^2 &= -(3{\cdot}181412\mu_1 + 3{\cdot}493635\mu_2), \qquad r_2 = 0, \\ \omega_1 &= 0{\cdot}426596 + 1{\cdot}413395\mu_1 + 0{\cdot}840417\mu_2; \end{aligned} \tag{19}$$

(3) Hopf bifurcation solution (HB (II) with frequency ω_2):

$$\begin{aligned} r_1 &= 0, \qquad r_2^2 = -64{\cdot}191814\mu_1 + 67{\cdot}004380\mu_2, \\ \omega_2 &= 0{\cdot}479012 + 1{\cdot}389397\mu_1 - 0{\cdot}406458\mu_2; \end{aligned} \tag{20}$$

(4) quasi-periodic solution (2-D tori with frequencies ω_1, ω_2):

$$r_1^2 = 26{\cdot}787429\mu_1 - 34{\cdot}775561\mu_2,$$

$$r_2^2 = -64{\cdot}191814\mu_1 + 67{\cdot}004380\mu_2,$$

$$\omega_1 = 0{\cdot}426596 + 0{\cdot}956895\mu_1 + 1{\cdot}316918\mu_2,$$

$$\omega_2 = 0{\cdot}479012 + 1{\cdot}389397\mu_1 - 0{\cdot}406458\mu_2. \tag{21}$$

The Jacobian matrix of equation (16) takes the form

$$J = \begin{bmatrix} -0{\cdot}487023\mu_1 - 0{\cdot}534819\mu_2 - 0{\cdot}459252r_1^2 - 0{\cdot}071469r_2^2 & -0{\cdot}142939r_1r_2 \\ 0 & -0{\cdot}479012\mu_1 + 0{\cdot}5\mu_2 - 0{\cdot}022387r_2^2 \end{bmatrix}, \tag{22}$$

which can be used for the stability analysis of the above steady state solutions.

Evaluating the Jacobian (22) on the fundamental equilibrium solution (18) results in the stable region for the ES as

$$0{\cdot}487023\mu_1 + 0{\cdot}534819\mu_2 > 0 \quad \text{and} \quad 0{\cdot}479012\mu_1 - 0{\cdot}5\mu_2 > 0,$$

which can be written in a more convenient form,

$$\mu_2 > -0{\cdot}910631\mu_1 \quad \text{and} \quad \mu_2 < 0{\cdot}958024\mu_1. \tag{23}$$

The boundaries defined by equation (23) lead to two critical lines, one of these is

$$L_1 : \mu_2 = -0{\cdot}910631\mu_1 \quad (\mu_2 < 0{\cdot}958024\mu_1), \tag{24}$$

where a family of limit cycles bifurcates from the ES with the approximate solution HB(I) given in equation (19). The second critical line is described by

$$L_2 : \mu_2 = 0{\cdot}958024\mu_1 \quad (\mu_2 > -0{\cdot}910631\mu_1) \tag{25}$$

from which another family of limit cycles, given by the HB(II) solution (20), may occur.

It should be noted that the two critical bifurcation lines L_1 and L_2 are actually the two tangent lines to the curves g_1 and g_2, respectively (see Figure 3), which pass through the critical point P. Thus, the conditions given in equation (23) indeed define the stability region of the initial equilibrium (ES) in the neighbourhood of the critical point P.

Evaluating, now, the Jacobian matrix (22) on the Hopf bifurcation solution (19) results in the stability conditions

$$0{\cdot}479012\mu_1 - 0{\cdot}5\mu_2 > 0 \quad (0{\cdot}974046\mu_1 + 1{\cdot}069638\mu_2 < 0) \tag{26}$$

or

$$\mu_2 < 0{\cdot}958024\mu_1 \quad (\mu_2 < -0{\cdot}910631\mu_1) \tag{27}$$

for the HB(I) solution. However, we should check whether the HB(I) solution exists under the conditions given in equation (26). Note that the condition $0{\cdot}974046\mu_1 + 1{\cdot}069638\mu_2 < 0$

implies that $3{\cdot}181412\mu_1 + 3{\cdot}493635\mu_2 < 0$, which indeed guarantees $r_1^2 > 0$ (see equation (19)) and thus stable periodic solutions exist in the region defined by equation (26).

The inequality given in equation (27) implies another critical line,

$$L_3\colon \mu_2 = 0{\cdot}958024\mu_1 \quad (\mu_2 < -0{\cdot}910631\mu_1), \tag{28}$$

along which a secondary Hopf bifurcation with frequency ω_2 takes place from the first bifurcating limit cycle HB(I), leading to a 2-D torus described by solution (21). However, it is noted that the critical lines L_2 and L_3 are located on a same straight line.

Similarly, a set of stability conditions associated with the HB(II) solution (20) can be derived by evaluating the Jacobian (22) on this solution. Thus, for the HB(II) solution to be stable, the inequalities

$$0{\cdot}958024\mu_1 - \mu_2 < 0 \quad \text{and} \quad 4{\cdot}100723\mu_1 - 5{\cdot}323577\mu_2 < 0 \tag{29}$$

must be satisfied. The first inequality in equation (29) is always satisfied when the parameters μ_1 and μ_2 are varied to cross the critical line L_2 from the stable region of the equilibrium.

To check if an HB(II) solution exists in the region defined by equation (29), we may rewrite the HB(II) solution as

$$r_2^2 = -64{\cdot}191814\mu_1 + 67{\cdot}004380\mu_2 = -67{\cdot}004380\,(0{\cdot}958024 - \mu_2),$$

which is guaranteed positive under condition (29). Hence, the HB(II) solution exists in the region defined by equation (29).

The second inequality of equation (29) defines a critical line,

$$L_4\colon \mu_2 = 0{\cdot}770295\mu_1 \quad (\mu_2 > 0{\cdot}958024\mu_1), \tag{30}$$

where a secondary Hopf bifurcation with frequency ω_1 takes place from the first bifurcating limit cycle HB(II), leading to a same family of 2-D tori described by solution (21).

Next, to find the stability of the family of 2-D tori expressed by equation (21), we evaluate the Jacobian (22) on equation (21) to get

$$J_{2-\mathrm{D\,tori}} = \begin{bmatrix} -0{\cdot}306168r_1^2 & -0{\cdot}142939r_1r_2 \\ 0 & -0{\cdot}014924r_2^2 \end{bmatrix}. \tag{31}$$

The stability conditions are then obtained from the trace and determinant of the Jacobian as follows:

$$\begin{aligned} \mathrm{Tr} &= -(0{\cdot}306168r_1^2 + 0{\cdot}014924r_2^2) \\ &= -7{\cdot}243421\mu_1 + 9{\cdot}647153\mu_2 \\ &= 9{\cdot}647153(\mu_2 - 0{\cdot}750835\mu_1) < 0, \\ \mathrm{Det} &= 0{\cdot}004569r_1^2r_2^2 \\ &= (-8{\cdot}201446\mu_1 + 10{\cdot}647153\mu_2)(0{\cdot}958024\mu_1 - \mu_2) \\ &= -10{\cdot}647153(\mu_2 - 0{\cdot}770295\mu_1)(\mu_2 - 0{\cdot}958024\mu_1) > 0. \end{aligned} \tag{32}$$

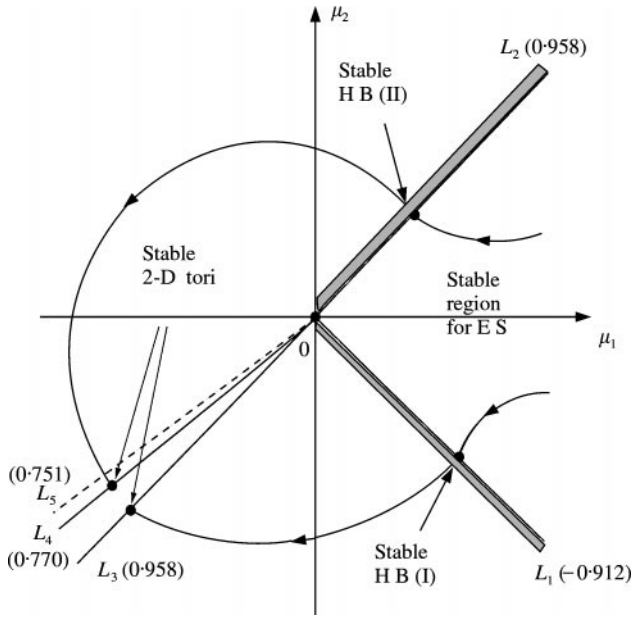

Figure 5. Bifurcation diagram for double-Hopf bifurcation.

It is easy to see that the two inequalities given in equation (32) are automatically satisfied as long as a solution (r_1, r_2) exists for a motion on the 2-D torus. For the existence of a quasi-periodic solution (on a 2-D torus), given by equation (21), it is required that

$$\mu_2 < 0{\cdot}770295\mu_1 \quad \text{and} \quad \mu_2 > 0{\cdot}958024\mu_1. \tag{33}$$

In fact, the boundaries defined by equation (33) are indeed the critical lines L_3 and L_4. Also, note that the conditions given in equation (33) guarantee that the second condition for the stability of the 2-D torus, given in equation (32), is satisfied. Moreover, it is noted that in the third quadrant of the $\mu_1 - \mu_2$ parameter space, the condition $\mu_2 < 0{\cdot}770295\mu_1$ implies that $\mu_2 - 0{\cdot}750835\mu_1 < 0$. Thus, the first condition for the stability of the 2-D torus (see equation (32)) is also satisfied, and so the family of 2-D tori is stable in the region defined by the existence condition (33).

Finally, note that the first inequality given in equation (32) yields a critical line,

$$L_5 \colon \mu_2 - 0{\cdot}750835\mu_1 = 0, \tag{34}$$

from which a quasi-periodic solution (2-D torus) loses stability and bifurcates into a motion n a 3-D torus $(\omega_1, \omega_2, \omega_3)$. However, this critical line is not located in the region defined by equation (33) and therefore, this tertial bifurcation cannot occur physically.

The bifurcation diagram for Model (III) is shown in Figure 5, where critical bifurcation lines are illustrated.

4. NUMERICAL METHODS

In this section, the numerical integration schemes to be used to verify the analytical results obtained in the previous two sections are discussed.

4.1. THE EXPLICIT RK4 METHOD

The RK4 method is a standard numerical integration procedure (see reference [22]), and thus we will not discuss the method here. The program we coded is flexible for changing the integration time step. However, the time step is fixed for each numerical experiment (so that we can compare the robustness of RK4 and the GS1 methods). A fixed time step of $\ell = 0{\cdot}1$ was chosen ($< 0{\cdot}1$ if the time step limit is less than 0·1) unless when we want to find the time step limit for the numerical scheme. The results are given below for the equilibrium and each of the three models separately. For the consistency in comparison, the original differential equation (3) is chosen for the numerical integration, and the initial condition is fixed as $\mathbf{z} = (0{\cdot}5, 0{\cdot}5, 0{\cdot}5, 0{\cdot}5, 0{\cdot}5)$. Furthermore, we will measure the solution $\mathbf{y}$ from the equilibrium $\mathbf{z}_c$ which is given by equation (4). In other words, the results presented in this section are for $\mathbf{y} = \mathbf{z} - \mathbf{z}_c$. Also, the associated central processing unit time (CPU) of the two numerical methods will be compared.

4.1.1. *For the equilibrium*

The close-form stability conditions for the equilibrium $\mathbf{y} = \mathbf{0}$ are given in equations (7) and (8), which define the stable region shown in Figure 3. Numerous simulations, using a number of points given in the (A, B) space located in the stable region, boundaries and unstable region, were carried out. Note that most of the points were chosen from the first quadrant (which is the region of interest). Few points were chosen from the third quadrant for testing purposes. It is expected that the numerical integration history will show convergence for a point chosen from the stable region. However, it will be shown that for a large time step, the RK4 method shows divergence even for a point chosen from the stable region (hence, the method failed). The results are given in Table 2, where TSUL = time step upper limit, denoting that the solution, which should be convergent or non-divergent, becomes divergent if the time step of the RK4 is greater than TSUL. "Convergent" means that the numerical solution converges to the true fixed-point $\mathbf{0}$, and "divergence" denotes that the whole solution (all the five components) or part of the solution (some of the five components) diverges to ∞. The interval given for the points chosen from stability boundary indicates that all the five components of the solution do not converge to $\mathbf{0}$, nor diverge to ∞, but wander in the vicinity of $\mathbf{0}$ bounded by the interval, implying that the points is indeed a critical point where $\mu = 0$.

4.1.2. *For Model (I)*

For this Model, we have simulated the RK4 program for several combinations of A and B and used the formula given in equation (10) to obtain the following analytical predictions:

(1) $A = 1{\cdot}0$.

(a) $B = 2{\cdot}5$ ($\mu = 0{\cdot}5$) and $r \approx 1{\cdot}1547$,

(b) $B = 3{\cdot}0$ ($\mu = 1{\cdot}0$) and $r \approx 1{\cdot}6330$.

(2) $A = 2{\cdot}0$.

(a) $B = 5{\cdot}5$ ($\mu = 0{\cdot}5$) and $r \approx 1{\cdot}8257$,

(b) $B = 6{\cdot}0$ ($\mu = 1{\cdot}0$) and $r \approx 2{\cdot}5820$.

The numerical simulation results for the above four cases are shown in Figure 6, where only the components y_1 and y_2 are shown since the two variables represent the first oscillator.

TABLE 2

*RK*4 *results for the equilibrium*

A	B	Region (analytic)	Result (numeric)	CPU time (s)	TSUL
0·5	1·24	Stable	Convergent	0·30	1·54
	0·90	Unstable	Divergent		
	1·25	Boundary g_1	[− 0·0016, 0·0082]	27·92	1·53
	1·210679	Boundary g_5	[− 0·0056, 0·0069]	3·60	1·58
0·8	1·50	Stable	Convergent	0·03	1·57
	0·80	Unstable	Divergent		
	1·64	Boundary g_1	[− 0·0000, 0·0000]	0·29	1·41
	1·001074	Boundary g_5	[− 0·0000, 0·0000]	0·17	1·39
1·0	1·50	Stable	Convergent	0·02	1·25
	0·70	Unstable	Divergent		
	2·00	Boundary g_1	[− 0·0003, 0·0003]	2·18	0·60
	0·903478	Boundary g_5	[− 0·0000, 0·0000]	2·11	1·41
2·0	3·00	Stable	Convergent	0·03	0·082
	0·60	Unstable	Divergent		
	5·00	Boundary g_1	[− 0·0095, 0·0078]	41·72	0·02
	0·632296	Boundary g_5	Divergent		0·00001
− 1·0	− 1·00	Stable	Convergent	0·00	1·21
0·0	− 1·00	Boundary g_5	Divergent		0·00001
− 1·0	0·00	Boundary g_5	Divergent		0·00001
− 1·0	1·00	Unstable	Divergent		
1·0	− 1·00	Unstable	Divergent		

Comparing the amplitudes given in the figure with the above analytical predictions shows that the numerical results obtained using RK4 method agree very well with the analytical results.

4.1.3. *For Model* (*II*)

Similarly, we have considered several cases and applied the formulae given in Table 1 to obtain the following analytical predictions:

(1) $A = 1{\cdot}0$.

(a) $B = 0{\cdot}803478$ ($\mu = -0{\cdot}10$) and $r \approx 1{\cdot}7353$,

(b) $B = 0{\cdot}753478$ ($\mu = -0{\cdot}15$) and $r \approx 2{\cdot}1253$.

(2) $A = 2{\cdot}0$.

(a) $B = 0{\cdot}612296$ ($\mu = -0{\cdot}02$) and $r \approx 0{\cdot}4089$,

(*b*) $B = 0{\cdot}602296$ ($\mu = -0{\cdot}03$) and $r \approx 0{\cdot}5009$.

The numerical simulation results for the above four cases are shown in Figures 7 and 8. It is noted that unlike Model(I), this Model has three non-zero variables y_3, y_4 and y_5 even though the first two variables, y_1 and y_2, always converge to the equilibrium. Thus, in the two figures, for each case, we show the limit cycles in three different co-ordinate systems: $y_3 - y_4$, $y_3 - y_5$ and $y_4 - y_5$ for a clear comparison with the analytical predictions. Also, it

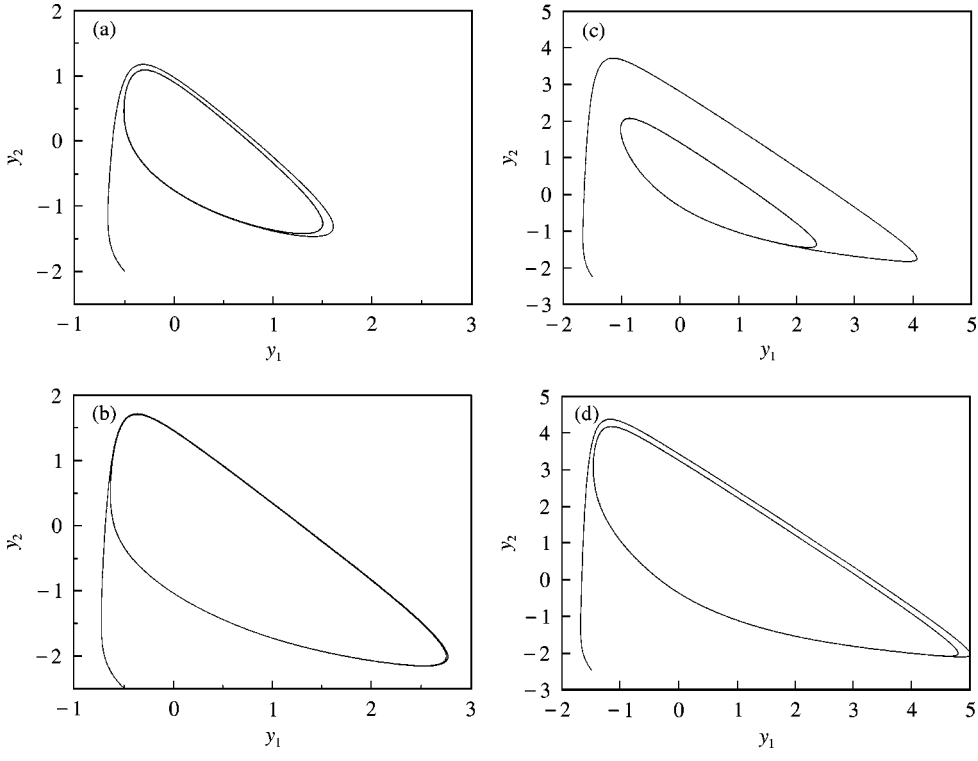

Figure 6. Limit cycles for Model (I): (a) $A = 1{\cdot}0$, $B = 2{\cdot}5$; (b) $A = 1{\cdot}0$, $B = 3{\cdot}0$; (c) $A = 2{\cdot}0$, $B = 5{\cdot}5$; (d) $A = 2{\cdot}0$, $B = 6{\cdot}0$.

has been noted that, unlike Model(I), where μ can be chosen to be quite large, here μ must be chosen to be very small, but the amplitudes of the limit cycles are still large. Additionally, it was observed that when the value of A is chosen far away from the critical point P (see Figure 3), the periodic solution is very sensitive to the initial conditions and the integration time step. In order to obtain stable limit cycles for the four cases, very small time steps must be chosen, in particular, for the case of $\mu = -0{\cdot}15$ of Figure 7 and the two cases given in Figure 8. Moreover, initial conditions must be chosen to be very close to the (unstable) equilibrium for the two cases shown in Figure 8. Otherwise, the solutions would not converge to a stable periodic solution. Using $A = 1$, the numerical results (see Figure 7) obtained show a good agreement with the analytical predictions, while for $A = 2$, the analytical results are smaller (in magnitude) than the numerical results (see Figure 8).

4.1.4. *For Model (III)*

Finally, for Model(III), we consider the following three cases, where the analytical predictions are obtained by using equations (19)–(21):

(1) $A = 0{\cdot}4790$, $B = 1{\cdot}1295$, i.e., $\mu_1 = 0{\cdot}0$, $\mu_2 = -0{\cdot}10$; this gives stable periodic solution (Hopf I), with $r_1 = 0{\cdot}5911$, $r_2 = 0$.
(2) $A = 0{\cdot}4790$, $B = 1{\cdot}3295$, i.e., $\mu_1 = 0{\cdot}0$, $\mu_2 = 0{\cdot}10$, this gives stable periodic solution (Hopf II), with $r_1 = 0$, $r_2 = 2{\cdot}5885$;
(3) $A = 0{\cdot}4390$, $B = 1{\cdot}1975$, i.e., $\mu_1 = -0{\cdot}04$, $\mu_2 = -0{\cdot}032$, this gives stable quasi-periodic solution (2-D tori), with $r_1 = 0{\cdot}2033$, $r_2 = 0{\cdot}6508$.

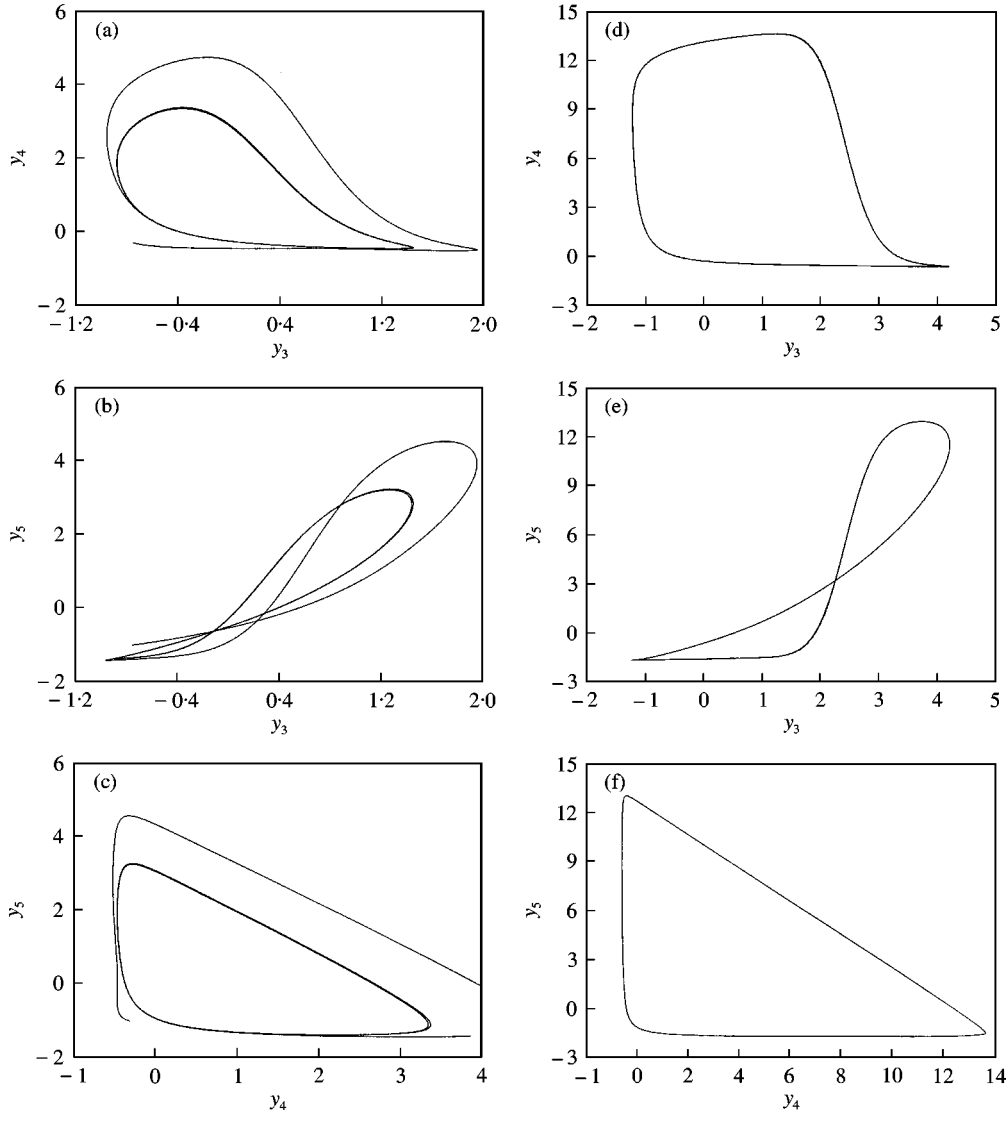

Figure 7. Limit cycles for Model (II) when $A = 1{\cdot}0$: for $\mu = -0{\cdot}10$, (a) y_3–y_4 plane; (b) y_3–y_5 plane; (c) y_4–y_5 plane; for $\mu = -0{\cdot}15$, (d) y_3–y_4 plane; (e) y_3–y_5 plane; (f) y_4–y_5 plane.

Here, it should be pointed out that the Hopf (I) and Hopf (II) bifurcation solutions do not correspond, respectively, to the first and second oscillators. These two combined modes are associated with frequencies $\omega_{1c} = 0{\cdot}426596$ and $\omega_2 = 0{\cdot}479012$ respectively (see equation (37)). The numerical results for the Hopf (I), Hopf (II) and 2-D tori are depicted in Figure 9(a), (b) and (c) respectively. In these figures, we only presented the solutions in the y_3–y_4 plane since figures in other planes are similar. It is noted that for the Hopf (I) bifurcation solution, $y_1 = y_2 = 0$. This is not surprising since one may use a linear transformation to show that the first two components y_1 and y_2 must be zero since $r_1 \neq 0$ and $r_2 = 0$. For the Hopf (II) and 2-D tori solutions, all the components of $\mathbf{y}$ are non-zero.

In order to clearly show the stable quasi-periodic solution on a two-dimensional torus, the trajectory y_i in the five-dimensional state space is projected on to the plane $y_3 = 0$ and

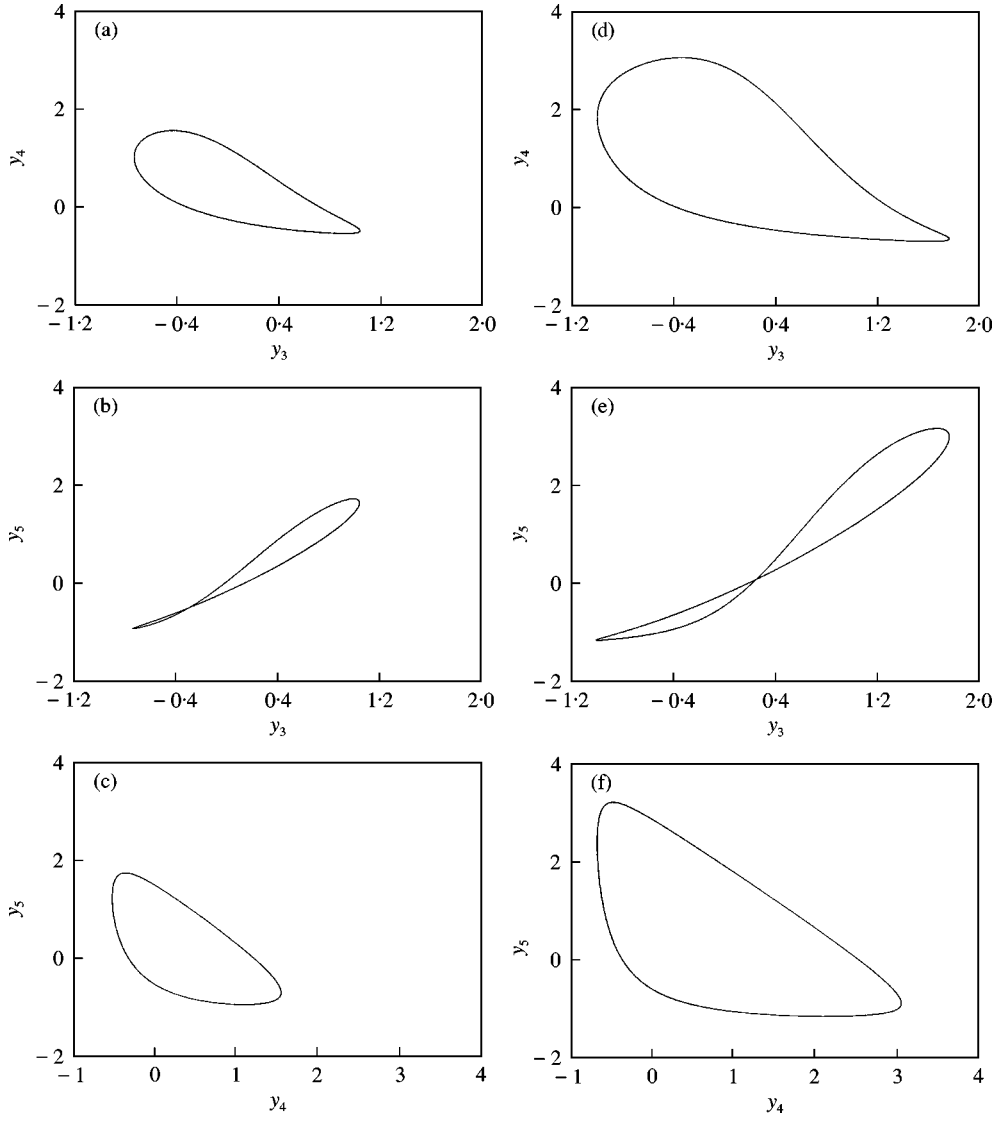

Figure 8. Limit cycles for Model (II) when $A = 2{\cdot}0$: for $\mu = -0{\cdot}02$, (a) y_3–y_4 plane; (b) y_3–y_5 plane; (c) y_4–y_5 plane; for $\mu = -0{\cdot}03$, (d) y_3–y_4 plane; (e) y_3–y_5 plane; (f) y_4–y_5 plane.

the half-plane $y_1 = 0,\ y_2 > 0$, respectively, to obtain two Poincaré maps as shown in Figure 10. Since the Poincaré maps are dense periodic orbits, the solution is indeed a quasi-periodic motion on a 2-D torus.

4.2. IMPLICIT METHOD: GS1

Having noted the severe stability limitation associated with the use of the explicit RK4 method for solving the IVP (6), there is clearly a need for an easy-to-use numerical method with enhanced stability properties. One such method is constructed below [23].

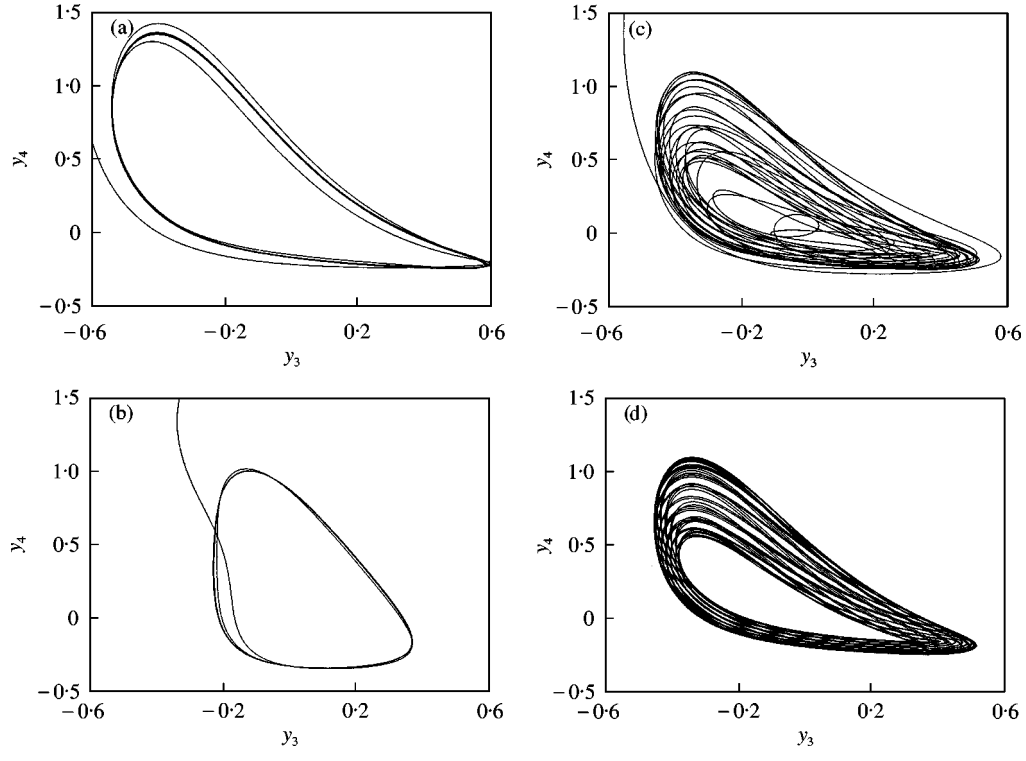

Figure 9. Simulation results for Model (III): (a) Hopf (I), $\mu_1 = 0{\cdot}0$, $\mu_2 = -0{\cdot}1$; (b) Hopf (II), $\mu = 0{\cdot}0$, $B = 0{\cdot}1$; (c) 2-D torus, $\mu_2 = -0{\cdot}04$, $\mu_2 = -0{\cdot}032$; (d) stable 2-D torus.

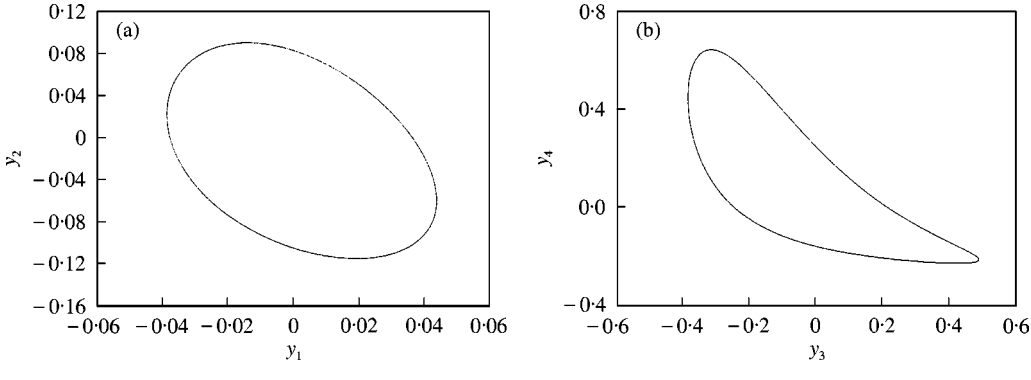

Figure 10. Poincaré maps of a 2-D torus for Model (III): (a) projected on to $y_3 = 0$ plane; (b) projected on to y_1–y_2 plane.

4.2.1. *Method for* z_1

Starting with the initial-value problem for z_1 given in equation (3) is expressed as

$$\dot{z}_1 \equiv \frac{\mathrm{d}z_1}{\mathrm{d}t} = A - Bz_1 + z_1^2 z_2 - z_1, \quad t > 0, \quad z_1(0) = Z^0, \tag{35}$$

the development of numerical methods may be based on the approximation of the time derivative in equation (35) by its first order forward-difference approximant

given by

$$\frac{dz_1}{dt} = \frac{z_1(t+\ell) - z_1(t)}{\ell} + O(\ell) \quad \text{as} \quad \ell \to 0, \tag{36}$$

where $\ell > 0$ is an increment in t (the time step). Discretizing the interval $t \geqslant 0$ at the points $t_n = n\ell$ $(n = 0, 1, 2, \ldots)$, the solution of equation (35) at the grid point t_n is $z_1(t_n)$. The solution obtained by a numerical method at the point t_n will be denoted by Z_1^n. Using equation (36) in equation (35) and approximating the right-hand side functions appropriately gives

$$Z_1^{n+1} = Z_1^n + \ell(A - BZ_1^{n+1} + Z_1^n Z_1^{n+1} Z_2^n - Z_1^{n+1}). \tag{37}$$

4.2.2. *Method for* z_2, z_3, z_4, z_5

Similarly, replacing the time derivatives for z_2, z_3, z_4 and z_5 in equation (3), using equation (36) and using appropriate approximations for their right-hand side functions, lead to

$$\begin{aligned}
Z_2^{n+1} &= Z_2^n + \ell[BZ_1^{n+1} - (Z_1^{n+1})^2 Z_2^{n+1}],\\
Z_3^{n+1} &= Z_3^n + \ell[Z_1^{n+1} - Z_3^{n+1} Z_4^n],\\
Z_4^{n+1} &= Z_4^n + \ell[BZ_1^{n+1} - Z_3^{n+1} Z_4^{n+1} + Z_4^n Z_4^{n+1} Z_5^n - Z_4^{n+1}],\\
Z_5^{n+1} &= Z_5^n + \ell[Z_3^{n+1} Z_4^{n+1} - (Z_4^{n+1})^2 Z_5^{n+1}].
\end{aligned} \tag{38}$$

It is easy to show that although the GS1 method, described by equations (37) and (38), is implicit by construction, equations (37) and (38) enable the IVP system (3) to be solved explicitly *via* the sequential process

$$Z_1^{n+1} = \frac{Z_1^n + \ell A}{1 + \ell(1 + B - Z_1^n Z_2^n)}, \qquad Z_2^{n+1} = \frac{Z_2^n + \ell BZ_1^{n+1}}{1 + \ell(Z_1^{n+1})^2}, \tag{39, 40}$$

$$Z_3^{n+1} = \frac{Z_3^n + \ell Z_1^{n+1}}{1 + \ell Z_4^n}, \qquad Z_4^{n+1} = \frac{Z_4^n + \ell BZ_1^{n+1}}{1 + \ell(1 - Z_4^n Z_5^n + Z_3^{n+1})} \tag{41, 42}$$

and

$$Z_5^{n+1} = \frac{Z_5^n + \ell Z_3^{n+1} Z_4^{n+1}}{1 + \ell(Z_4^{n+1})^2}. \tag{43}$$

It is an easy exercise to verify that the principal part of the local truncation error associated with each of the methods in equations (39)–(43) is of $O(\ell^2)$ confirming that the GS1 method is first order accurate (see also reference [23]).

4.2.3. *Numerical experiments*

To test the behaviour of the GS1 method, numerous simulations were carried out using various time steps with $A = 2$, $B = 1{\cdot}5$ and $Z_1(0) = Z_2(0) = Z_3(0) = Z_4(0) = Z_5(0) = 0{\cdot}5$. The convergence property of the GS1 method using various time steps was compared with those of some standard (well-known) methods in the literature and the results are tabulated in Table 3.

It is clear from Table 3 that GS1 is most competitive in terms of numerical stability. Expectedly, all the three explicit methods (Euler, RK2 and RK4) used in the simulations

TABLE 3

Convergence for methods Euler, RK2, RK4 and GS1

l	Euler	RK2	RK4	GS1
0·001	Converge	Converge	Converge	Converge
0·01	Converge	Converge	Converge	Converge
0·1	Converge	Diverge	Converge	Converge
0·2	Converge	Diverge	Converge	Converge
0·3	Diverge	Diverge	Converge	Converge
0·5	Diverge	Diverge	Diverge	Converge
1	Diverge	Diverge	Diverge	Converge
100	Diverge	Diverge	Diverge	Converge

TABLE 4

CPU time for GS1 and YK4

A	B	GS1	YK4
0·5	1·24	0·42	1·27
0·5	1·25	0·42	1·30
0·8	1·50	0·44	1·40
1·0	1·50	0·47	1·38
2·0	3·00	0·44	(Diverge)

failed when large time steps were used. This is consistent with the fact that implicit methods (and not explicit schemes) are most suited for solving non-linear IVPs such as equation (5).

In Table 4, we compare the CPU times of the RK4 and GS1 methods. For convenience of comparison, the time step is fixed at $\ell = 0{\cdot}1$, and the initial condition is again chosen as $Z_1(0) = Z_2(0) = Z_2(0) = Z_3(0) = Z_5(0) = Z_1(0) = 0{\cdot}5$. All the points (A, B) given in Table 4 are selected from the stable region of the equilibrium. Thus, the numerical results should show convergence for all the points. However, for the RK4 method, it indicates a divergence for $(A, B) = (2, 3)$, implying that the time step 0·1 is not small enough for this case when using RK4 method. It is worth emphasizing that all the numerical computations carried out for this paper were implemented on a PC machine (PENTIUM III-700MMX 256K system). The number of iterations used for the comparison is 50 000. It is clearly evident form Table 4 that the GS1 method only takes about one-third the CPU time of RK4, confirming that GS1 is more efficient computationally.

Next, we compare GS1 method with the RK4 approach for the dynamic solutions. Figure 11 shows the results for the equilibrium, Models (I) and (II), while Figure 12 gives the results for Model (III). Comparison of the results clearly indicates that GS1 and RK4 give roughly the same results. However, we already prove that the GS1 method is more robust than the RK4 method, in particular, for the convergence of the equilibrium.

In the above discussion, we have shown that the GS1 method gives almost the same accuracy as the RK4 does for many cases. In fact, we further observed that if a case (or a chosen point in the parameter space) is not very sensitive to the given initial condition, then the accuracy of GS1 is comparable with that of the RK4 for the same time step. The time steps used in the simulations shown in Figures 11 and 12 were: 0·1 for the equilibrium;

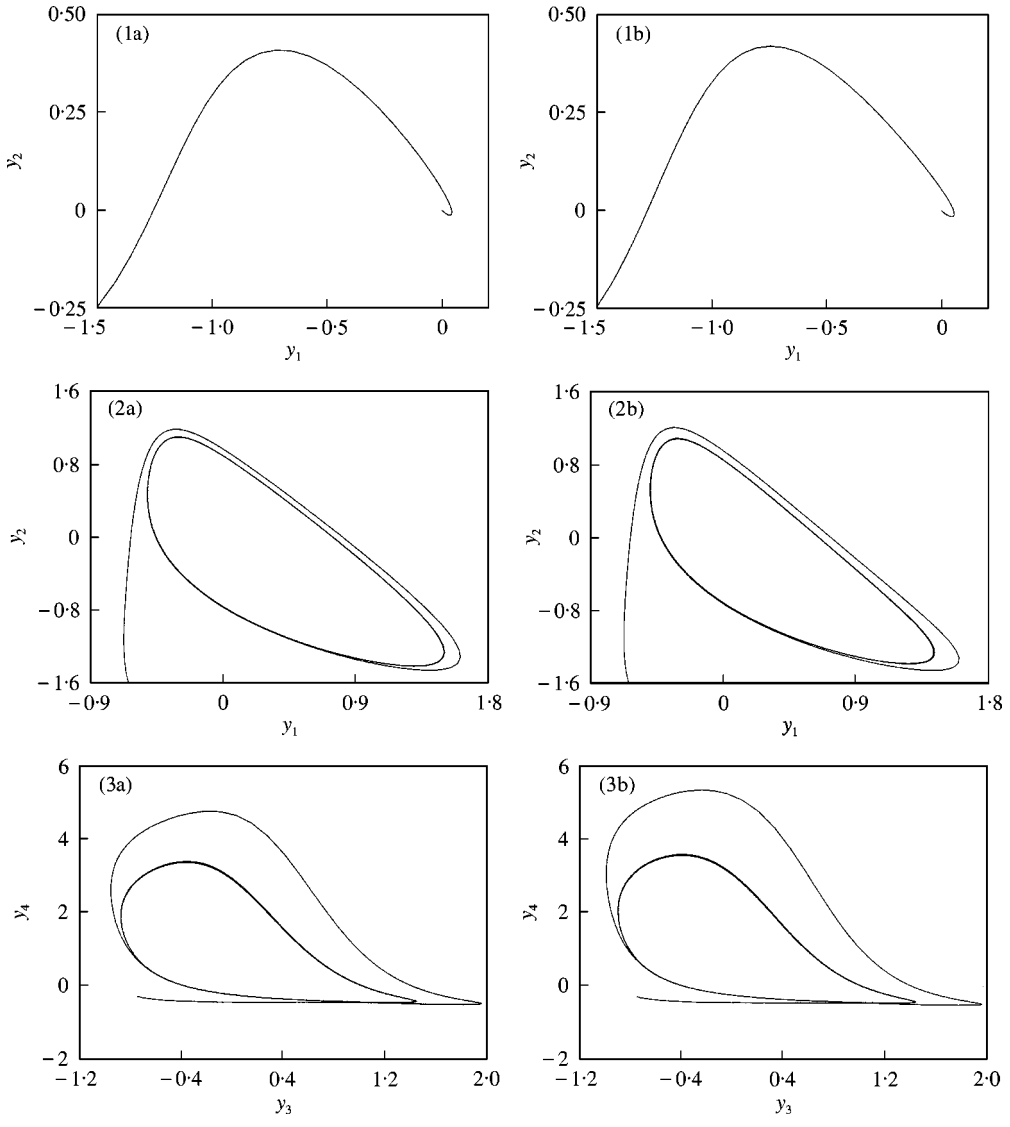

Figure 11. Comparison of RK4 (a) and GS1 (b) for (1) $A = 2{\cdot}0$, $B = 1{\cdot}5$: equilibrium; (2) $A = 2{\cdot}0$, $B = 2{\cdot}5$: Model (I); and (3) $A = 1{\cdot}0$, $B = 0{\cdot}803478$: Model (II).

0·05 for Model (I); 0·02 for Model (II); 0·1 for Model (III), Hopf (I) and Hopf (II); 0·02 for the two-dimensional torus. The same initial conditions were used in the numerical simulations to generate the results depicted in Figures 11 and 12 given by $z = (0{\cdot}5, 0{\cdot}5, 0{\cdot}5, 0{\cdot}5, 0{\cdot}5)$. However, it was found that the dynamical system was sensitive to the initial conditions used. For example, for the results obtained for Model (II) shown in Figure 8, the initial condition $\mathbf{z} = (0{\cdot}5, 0{\cdot}5, 0{\cdot}5, 0{\cdot}5, 0{\cdot}5)$ leads to a slowly diverging result irrespective of the size of the time step used. In fact, for the case $\mu = -0{\cdot}02$, i.e., $B = 0{\cdot}612296$, we must choose an initial condition near the orbit for convergence. For the case $\mu = -0{\cdot}03$, i.e., $B = 0{\cdot}602296$, even an initial condition close to the orbit does not work. It must be chosen almost on the orbit. The RK4 and GS1 methods were compared for the two cases as follows: for the case $\mu = -0{\cdot}02$, we chose the initial condition $\mathbf{z} = (2{\cdot}5, 0{\cdot}5, 1{\cdot}0, 1{\cdot}0, 1{\cdot}0)$ which is near the final

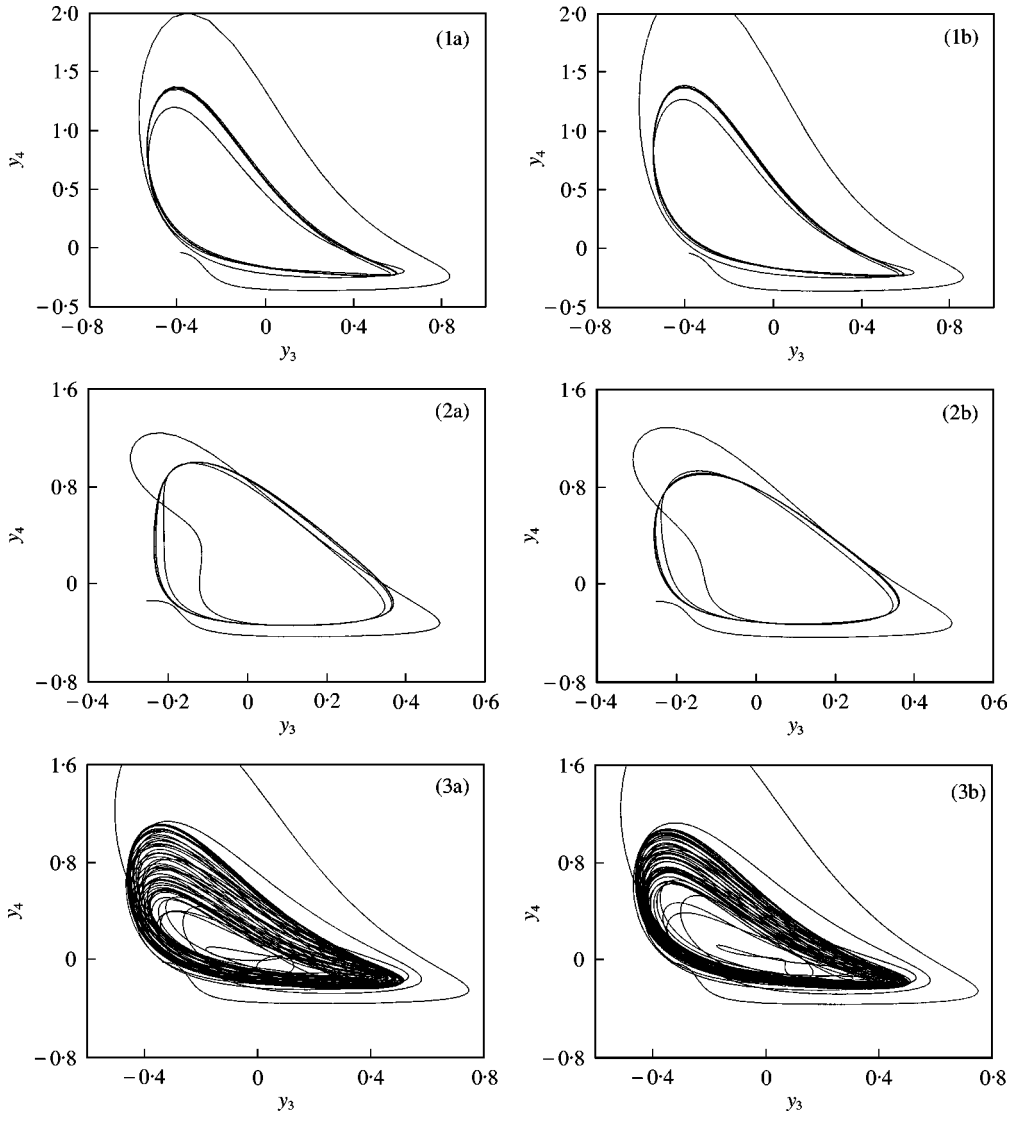

Figure 12. Comparison of RK4 (a) and GS1 (b) for Model (III) when (1) $A = 0{\cdot}4790$, $B = 1{\cdot}1295$: Hopf (I); (2) $A = 0{\cdot}4790$, $B = 1{\cdot}3295$: Hopf (II); (3) $A = 0{\cdot}4390$, $B = 1{\cdot}1975$: quasi-periodic motion on 2-D torus.

stable orbit, and found that the RK4 gives convergent results as long as the time step $\ell \leqslant 0{\cdot}83$, while GS1 give monotonically diverging results even for $\ell = 0{\cdot}000001$. For the case $\mu = -0{\cdot}03$, we chose the initial condition $\mathbf{z} = (2{\cdot}0,\ 0{\cdot}301148,\ 0{\cdot}896217,\ 1{\cdot}805416,\ 0{\cdot}400966)$ which is almost on the final stable orbit, we then found that the RK4 shows convergence if $\ell \leqslant 0{\cdot}36$, while GS1 gives divergent results even when $\ell = 0{\cdot}000001$.

Finally, we compared the two methods for the quasi-periodic motion on a two-dimensional torus. It is interesting to observe that, for this case, although the solution is not sensitive to the initial condition, different time steps do give different dynamical behaviour. For instance, using the initial condition $\mathbf{z} = (0{\cdot}5,\ 0{\cdot}5,\ 0{\cdot}5,\ 0{\cdot}5,\ 0{\cdot}5)$ and time steps $\ell \leqslant 0{\cdot}02$, it was found that both methods gave stable quasi-periodic motions. However, when the time step was increased to $\ell > 0{\cdot}02$, RK4 still shows stable quasi-periodic motion,

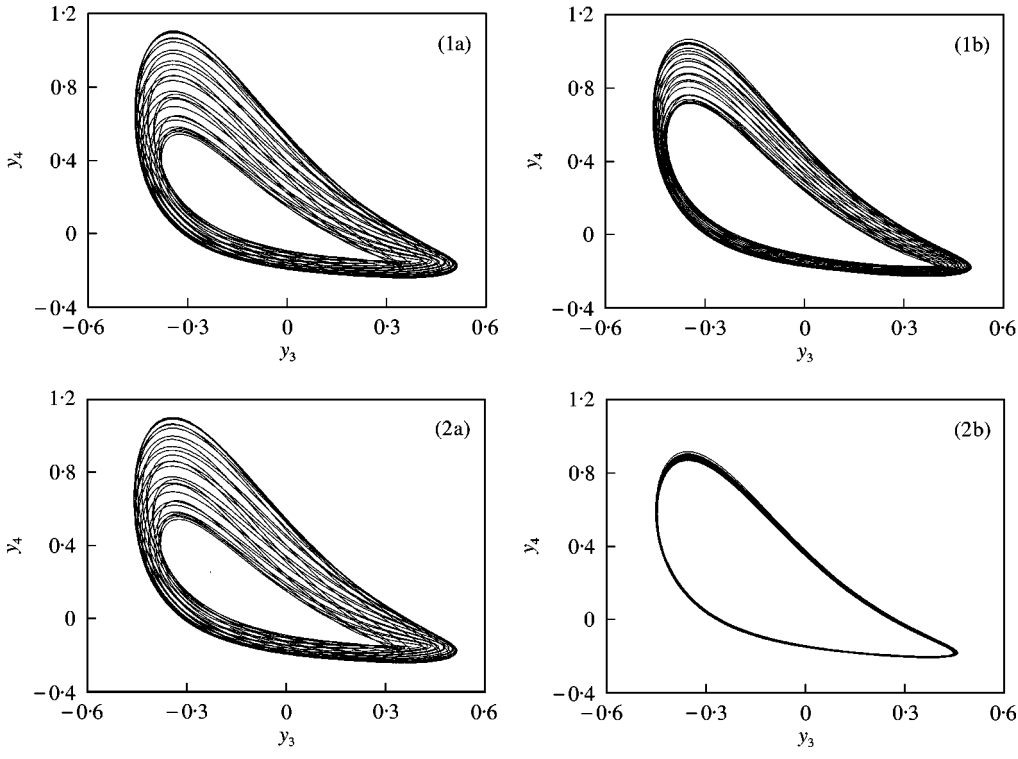

Figure 13. Comparison of RK4 (a) and GS1 (b) for Model (III) with different time steps when $A = 0{\cdot}4390$, $B = 1{\cdot}1975$: (1) $\ell = 0{\cdot}02$; (2) $\ell = 0{\cdot}08$.

while GS1 gives stable motion which is not quasi-periodic, but periodic. Two cases are shown in Figure 13, where the RK4 results are shown in the left column (a) and the GS1 results are given in the right column (b). The corresponding Poincaré maps are shown in Figure 14, which clearly indicate that for the GS1 method, when the time step equals 0·04, the quasi-periodic motion is degenerated to a periodic solution, since its Poincaré map is a point, not a closed orbit. It should be noted that the Poincaré maps are projected on to the y_1–y_2 plane since the results given by the GS1 method are degenerated to periodic solutions on the y_3–y_4 plane. Part (2b) in Figure 14 is actually just one point (0, 0). In fact, comparing part (2a) with (1a) indicates the degeneration of the method GS1 as the time step increases, while the RK4 method has almost no influence from the time step change. This is due to the fact that the GS1 method is only first order accurate, while the RK4 method is fourth order. The order has little influence on the convergence to an equilibrium, that is why the GS1 method is more robust than the RK4 method for the static analysis (see Table 3). For the dynamical analysis, on the other hand, a solution to the IVP problem converges to either periodic or quasi-periodic motions, so that it may be sensitive to initial conditions. In this case, the RK4 method is more robust than the GS1 method since it gives a more accurate solution due to its higher order.

5. CONCLUSIONS

A coupled Brusselator chemical system has been studied in detail to show its rich dynamic behaviour in the vicinity of three different types of critical points. Closed-form

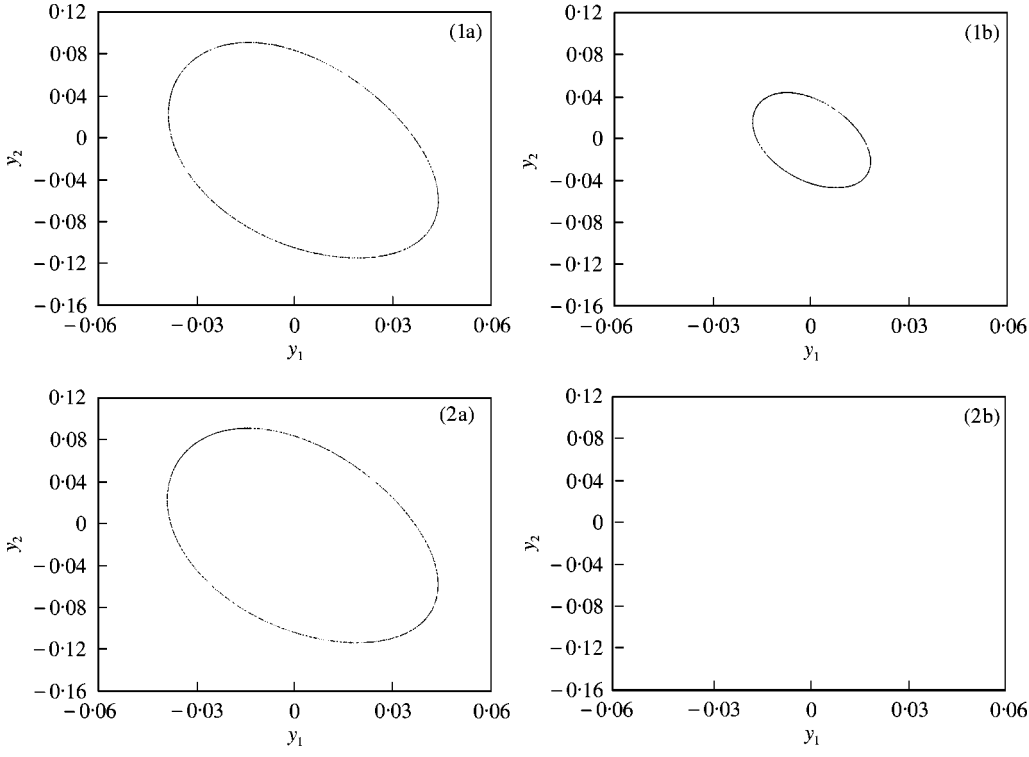

Figure 14. Poincaré maps for the comparison of RK4 (a) and GS1 (b) for Model (III) with different time steps when $A = 0{\cdot}4390$, $B = 1{\cdot}1975$: (1) $\ell = 0{\cdot}02$; (2) $\ell = 0{\cdot}08$.

solutions have been obtained, *via* bifurcation analysis, for periodic and quasi-periodic solutions. The stability conditions for the steady state solutions are also given explicitly in terms of the system parameters. Critical stability boundaries along which incipient and secondary bifurcations leading to periodic solutions and quasi-periodic motions on 2-D tori are also explicitly obtained. All the results are derived using the normal form theory and centre manifold theory. Two numerical approaches have been applied to confirm the analytical predictions. It is shown that the GS1 method and the fourth order Runge–Kutta method gave roughly the same results. But the first order GS1 method is more robust and takes less computation time. The coupled Brusselator may exhibit chaotic motions, which are not considered in this paper and will be reported in a separate article later.

ACKNOWLEDGMENTS

The authors gratefully acknowledge the support of the Natural Sciences and Engineering Research Council of Canada.

REFERENCES

1. R. LEFEVER and G. NICOLIS 1971 *Journal of Theoretical Biology* **30**, 267–284. Chemical instabilities and sustained oscillations.
2. G. NICOLIS and I. PRIGOGINE 1977 *Self-organizations in Non-equilibrium Systems*. New York: Wiley-Interscience.

3. J. TYSON 1972 *Journal of Chemical Physics* **58**, 3919–3930. Some further studies of non-linear oscillations in chemical systems.
4. G. ADOMIAN 1995 *Computers in Mathematical Applications* **29**, 1–3. The diffusion Brusselator equation.
5. J. GUCKENHEIMER 1984 *SIAM Journal of Mathematical Analysis* **15**, 1–49. Multiple bifurcations of codimension two.
6. J. GUCKENHEIMER and P. HOLMES 1993 *Nonlinear Oscillations, Dynamical Systems, and Bifurcations of Vector Fields*. New York: Springer-Verlag; fourth edition.
7. P. STEEN and S. H. DAVIS 1982 *SIAM Journal of Applied Mathematics* **42**, 1345–1368. Quasi-periodic bifurcation in non-linearly coupled oscillators near a point of strong resonance.
8. R. SCHEIDL, H. TROGER and K. ZEMAN 1984 *International Journal of Non-linear Mechanics* **19**, 163–176. Coupled flutter and divergence bifurcation of a double pendulum.
9. K. HUSEYIN 1986 *Multiple-Parameter Stability Theory and Its Applications*. Oxford: Oxford University Press.
10. K. HUSEYIN and P. YU 1988 *Applied Mathematical Modelling* **12**, 189–201. On bifurcations into nonresonant quasi-periodic motions.
11. P. YU and K. HUSEYIN 1993 *Quarterly Applied Mathematics* **51**, 91–100. On phase-locked motions associated with strong resonance.
12. S. SAMARANAYAKE and A. K. BAJAJ 1993 *Nonlinear Dynamics* **4**, 605–633. Bifurcation in the dynamics of an orthogonal double pendulum.
13. D. E. GILSINN 1993 *Nonlinear Dynamics* **4**, 289–308. Constructing invariant tori for two weakly coupled van der Pol oscillators.
14. P. YU and Q. BI 1998 *Journal of Sound and Vibration* **217**, 691–736. Analysis of non-linear dynamics and bifurcations of a double pendulum.
15. J. CARR 1981 *Applications of Center Manifold Theory*. New York: Springer-Verlag.
16. C. ELPHICH, E. TIRAPEGUI, M. E. BRACHET, P. COULLET and G. IOOSS 1987 *Physica D* **29**, 95–127. A simple global characterization for normal forms of singular vector fields.
17. S.-N. CHOW, C.-Z. LI and D. WANG 1994 *Normal Forms and Bifurcation of Planar Vector Fields*. Cambridge: Cambridge University Press.
18. A. H. NAYFEH 1993 *Methods of Normal Forms*. New York: John Wiley & Sons.
19. P. YU 1998 *Journal of Sound and Vibration* **211**, 19–38. Computation of normal forms via a perturbation technique.
20. Q. BI and P. YU 1999 *Mathematics and Computer Modelling* **29**, 49–70. Symbolic software development for computing the normal forms of double Hopf bifurcation.
21. S. ZHU and P. YU 1999 *Proceedings of 17th CANCAM*, 69–70. Computing normal forms for vibration analysis of nonlinear oscillators via multiple time scales.
22. C. F. GERALD and P. O. WHEATLEY 1994 *Applied Numerical Analysis*. New York: Addison-Wesley Publishers; fifth edition.
23. E. H. TWIZELL, A. B. GUMEL and Q. CAO 1999 *Journal of Mathematical Chemistry* **26**, 297–316. A second-order scheme for the Brusselator reaction–diffusion system.